Supplementary Information

Electrochemically plated nickel-decorated ceria nanostructures for direct hydrocarbon solid oxide fuel cell electrodes

Jinwook Kim[†,1], Yoonseok Choi[†,2], Dae-Kwang Lim[1], JeongDo Yoo[1], Han Gil Seo[3], Seunghyun Kim[1], Sangwoo Kim[1] and WooChul Jung[1]*

[1]Department of Materials Science and Engineering, Korea Advanced Insititute of Science and Technology (KAIST) 291 Daehak-ro, Yuseong-gu, Daejeon, 34141, Republic of Korea

[2]High Temperature Energy Conversion Laboratory, Korea Institute of Energy Research (KIER), Gajeong-ro, Yuseong-gu, Daejeon 34129, Republic of Korea

[3]Department of Materials Science and Engineering, Massachusetts Institute of Technology (MIT), 77 Massachusetts Avenue, Cambridge, MA, 02139, USA

*E-mail: wcjung@kaist.ac.kr, Phone: +82-42-350-3314, Fax: +82-42-35-3310

[+]Jinwook Kim and Yoonseok Choi contributed equally to this study.

JeongDo Yoo, Current address: Catalyst R&D, Catalyst Division, Petrochemicals Company, LG Chem Research Park, 188, Moonji-ro, Yuseong-gu, Daejeon, Republic of Korea

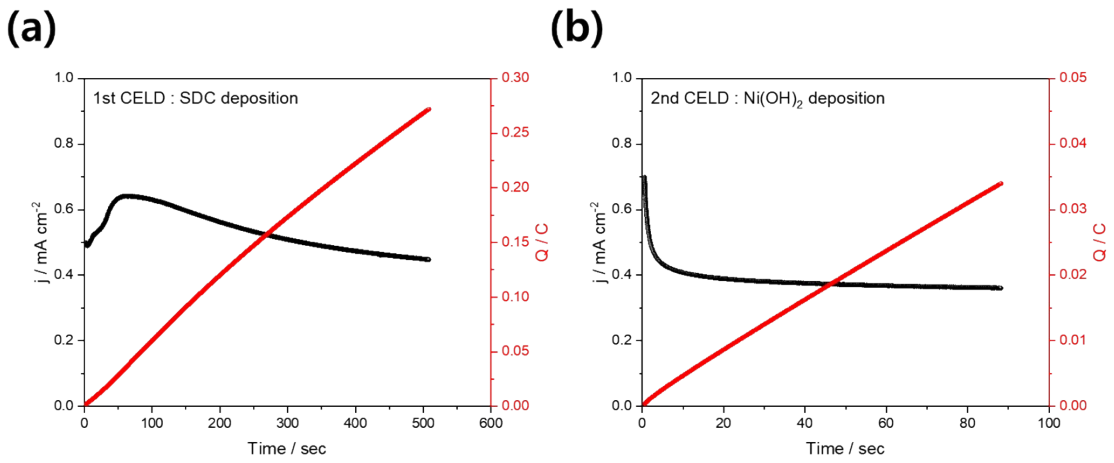

Figure S1. Double y-axes plot of current density (j)-time transients (left y-axis) and charge (Q)-time transients (right y-axis) for the 1st and 2nd CELD steps for 12 at% Ni NP-SDC composite nanostructures.

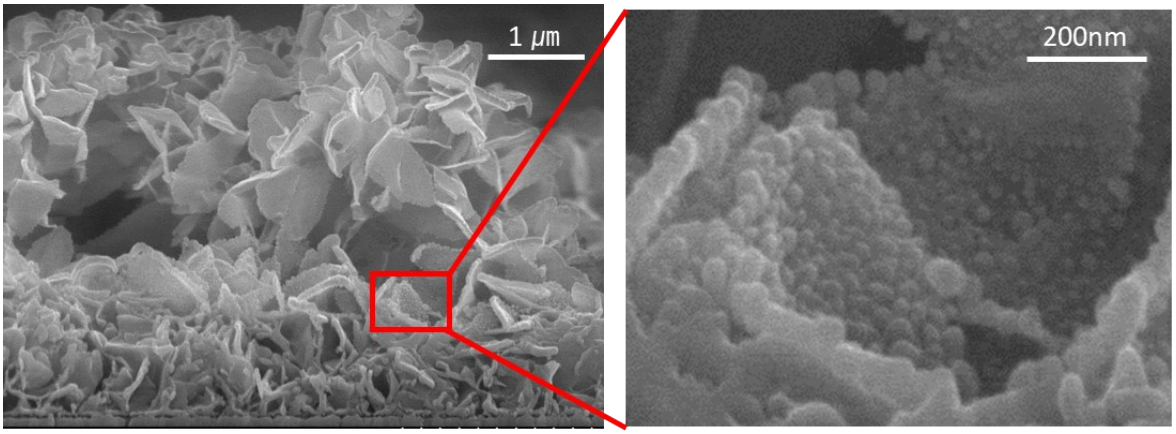

Figure S2. Cross-section SEM images of the surface morphology of the Ni NP-SDC composite nanostructures.

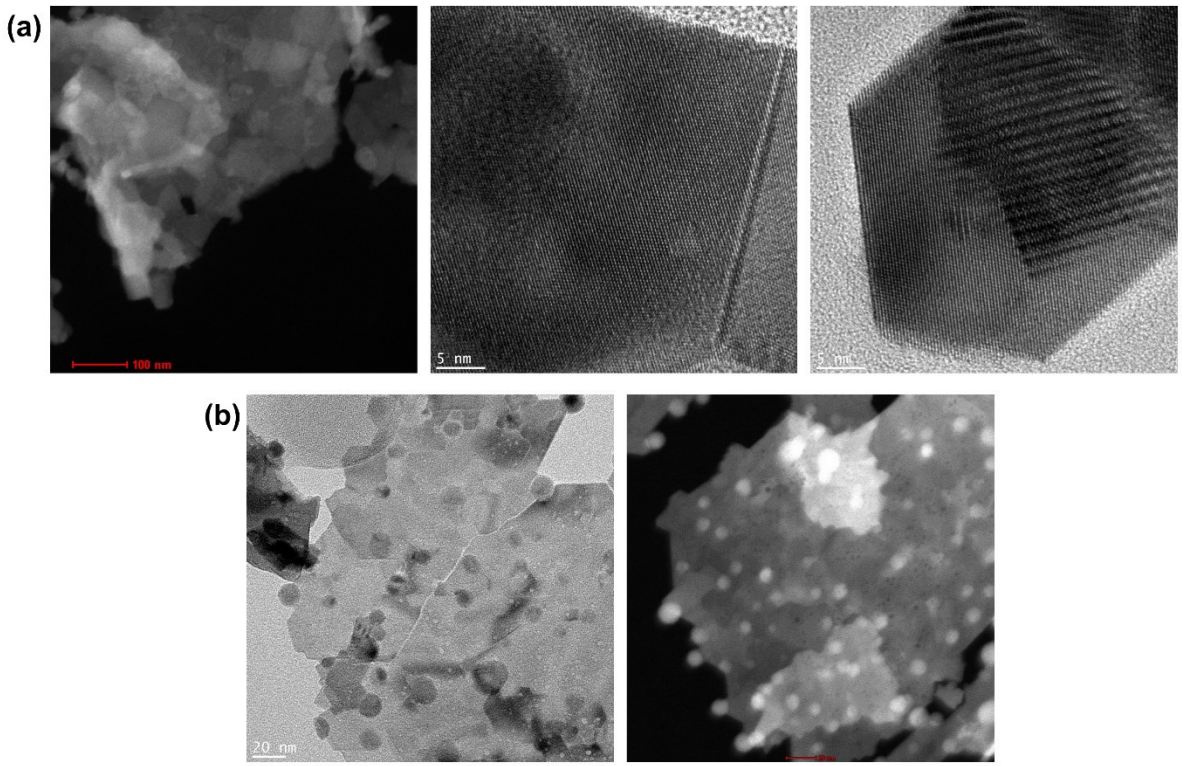

Figure S3. HAADF-STEM image of a scrapped nanosheet, (a) SDC CELD, (b) Ni NP-SDC CELD (12 at%).

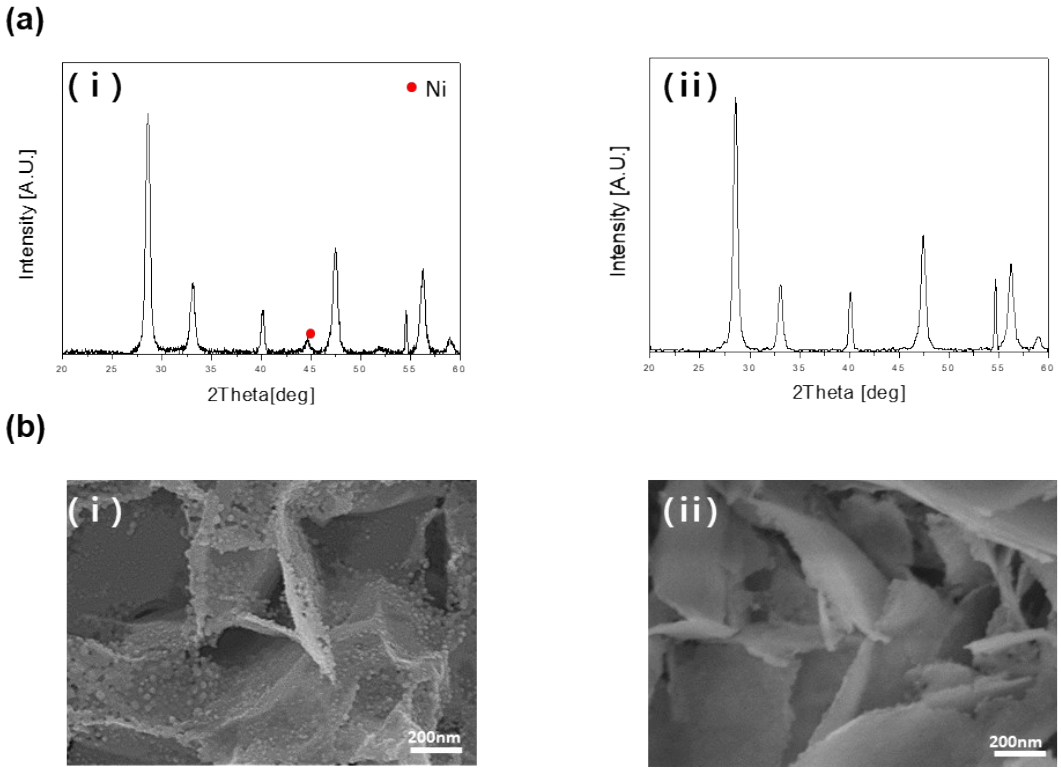

Figure S4. (a) XRD patterns of the Ni NP-SDC overcoat (i) before Ni etching and (ii) after etching, and (b) SEM images of the Ni NP-SDC overcoat (i) before Ni etching and (ii) after etching.

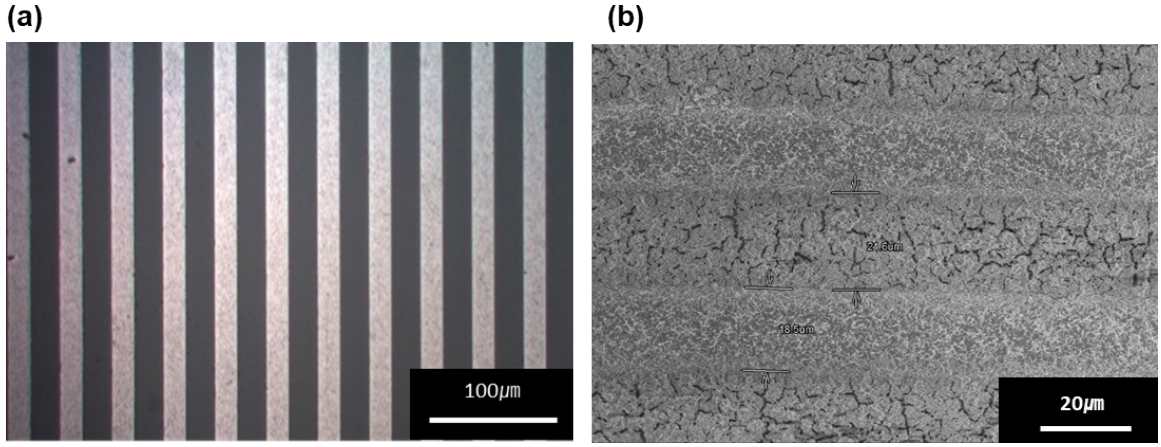

Figure S5. (a) OM image of strip Ni-YSZ model electrode where the width of Ni stripe and the Ni-to-Ni distance are 20 μm (l_{TPB} = 3.248 m cm^{-2}). (b) SEM image of Ni NP-SDC coated Ni-YSZ model electrode.

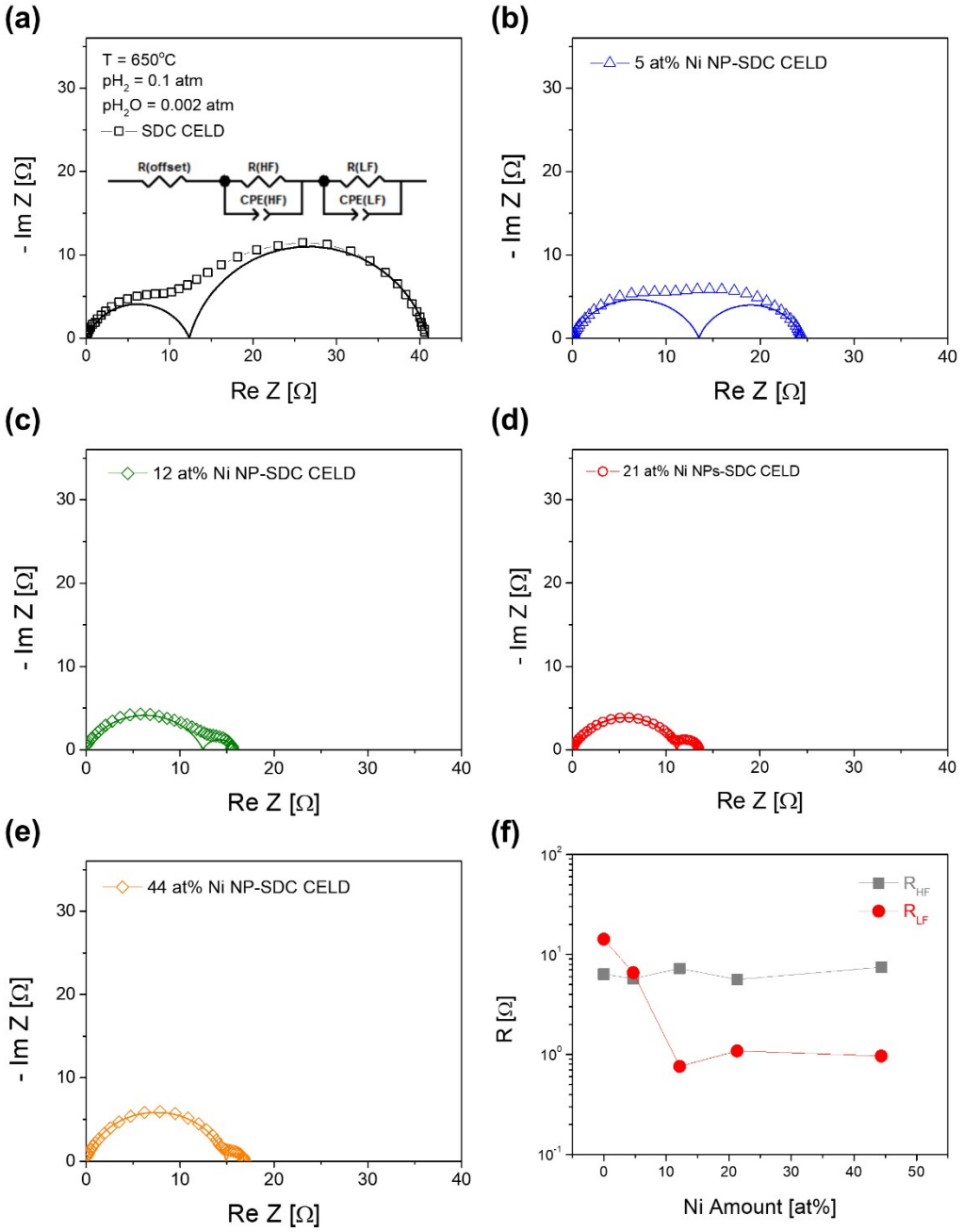

Figure S6. The fitting results of the impedance spectra obtained for the Ni NP-SDC CELD samples with an equivalent circuit model; R_{offset}-$R_{HF}Q_{HF}$-$R_{LF}Q_{LF}$ where Q is a constant phase element (CPE). A capacitance (C) in Figure S6, for example, can be calculated from the equation; $C = (R^{1-n}Q)^{1/n}$. R_{offset} was omitted for easy comparison. (a) 0 at%, (b) 5 at%, (c) 12 at%, (d) 21 at%, and (e) 44 at%. T = 650°C, pH_2 = 0.1 atm and pH_2O = (2.1±0.1) × 10^{-3} atm. (f) The summarized R_{HF} and R_{LF} values as a function of Ni amount, showing clearly that R_{HF} is largely independent of the secondary Ni CELD process.

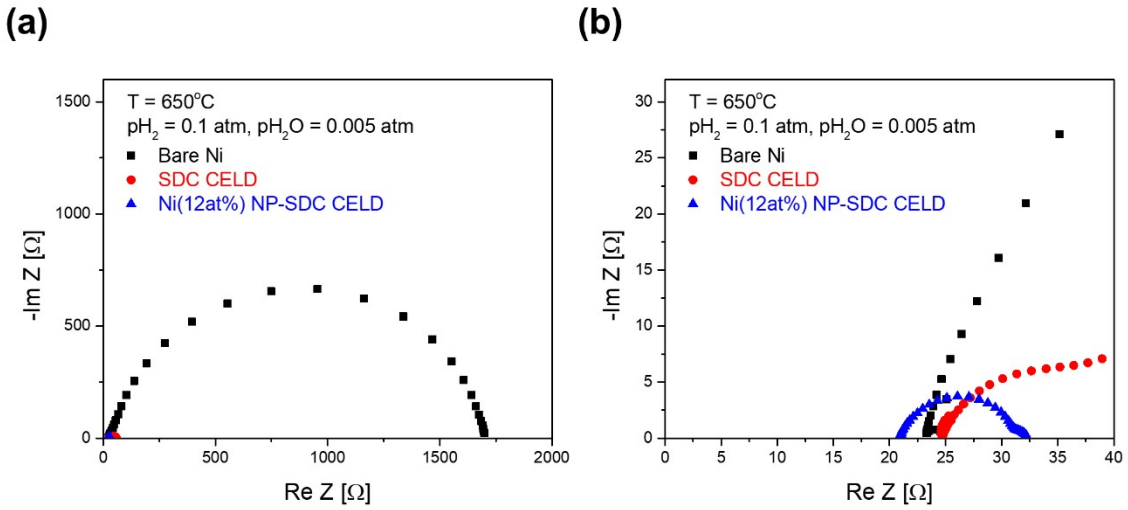

Figure S7. (a) The typical raw impedance spectra of the symmetric model Ni-YSZ without CELD (Bare Ni, black square), with SDC CELD (red circle), and with 12at% Ni NP-SDC CELD (blue triangle) obtained under wet H_2 ($10\%H_2$-$0.5\%H_2/N_2$) atmosphere at 650°C. (b) The magnified graph of the high-frequency region, showing the offset resistance (R_{offset}). The average of the R_{offset} is 25.8 ± 3.2 Ω without any trend towards subsequent CELD conditions. The average activation energy for the R_{offset} in temperature range between 550 and 650°C is 0.56 ± 0.02 eV.

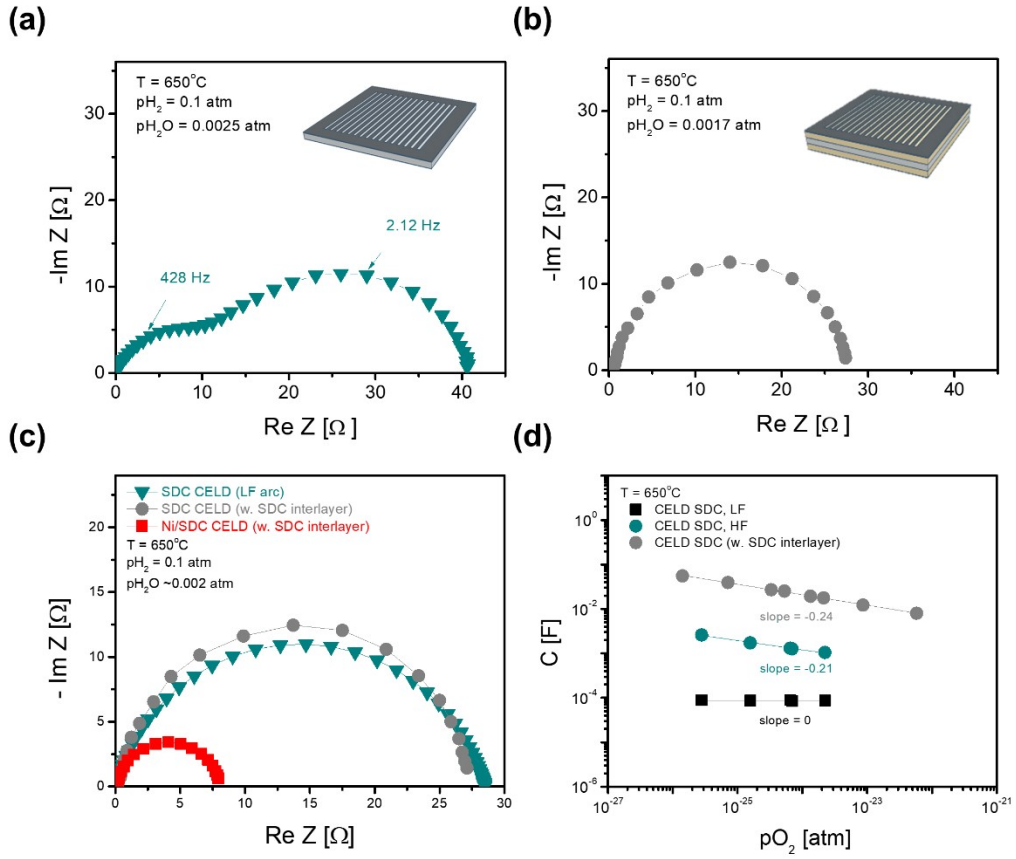

Figure S8. The typical impedance spectra of the SDC CELD samples (a) without and (b) with a dense PLD SDC interlayer. The offset resistance is omitted for easy comparison. The corresponding cell geometries are (a) patterned Ni‖YSZ‖patterned Ni, and (b) patterned Ni‖PLD SDC‖YSZ‖PLD SDC‖patterned Ni, respectively. (c) Fitted low-frequency arc of the impedance spectra of the SDC CELD samples without a PLD SDC interlayer (turquoise ▼), with a PLD SDC interlayer (gray ●), and Ni NP-SDC CELD with a PLD SDC interlayer (red ■). (d) Double logarithmic plot of the capacitance of SDC CELD without and with a dense PLD SDC interlayer.

Origin of high-frequency arc for Ni NP-SDC CELD samples: As discussed in the main text, the HF arc in the SDC or Ni NP-SDC CELD arises from 'constriction effect' due to the unique geometries of the patterned Ni-YSZ (Figure S7a) [1]. Meanwhile, this arc can be eliminated by inserting a dense SDC layer between patterned Ni and YSZ electrolyte (Figure S7b). Then, it was found that the remaining single arc behaves almost identically with the LF arc of the SDC CELD sample without a SDC layer, indicating the same origin, the electrochemical processes at the SDC/gas interfaces (Figure S7c and S7d).

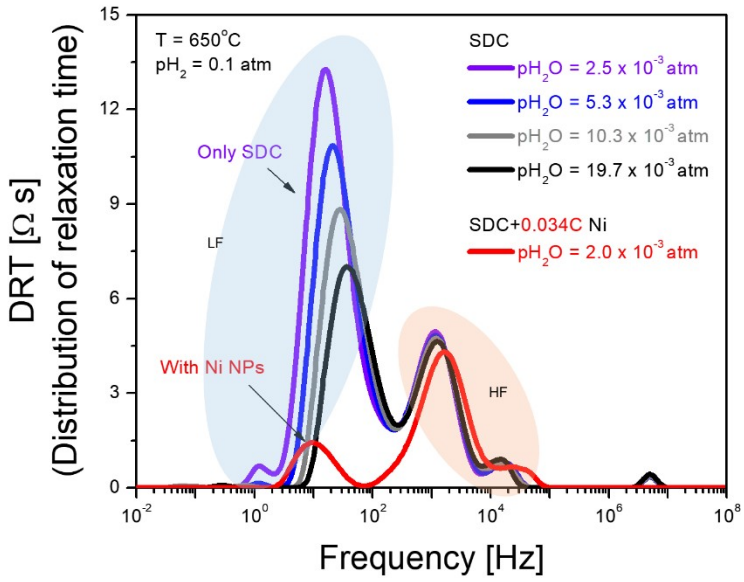

Figure S9. Distribution of relaxation times (DRT) plots of SDC CELD and Ni NP-SDC CELD of the symmetrical Ni-YSZ model electrode under wet H_2 (T = 650℃ and pH_2=0.1 atm)

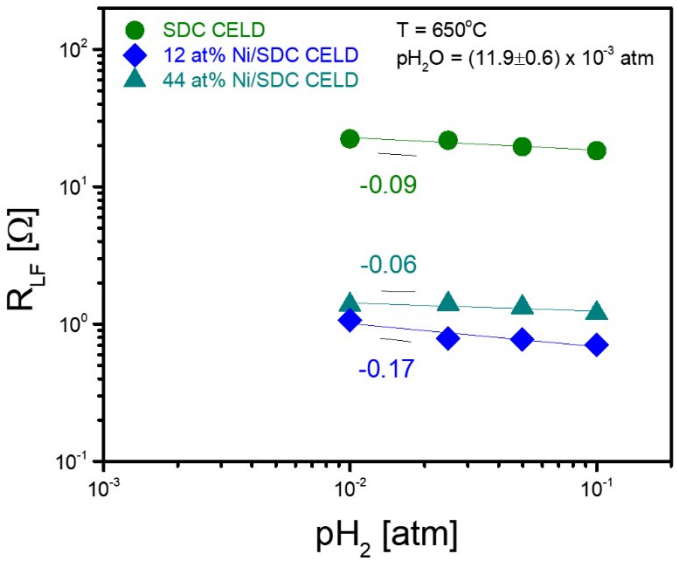

Figure S10. Double logarithmic plot of the R_{LF} of SDC CELD (green circle), 12 at% Ni NP-SDC (blue diamond) and 44 at% Ni NP-SDC (turquoise triangle) vs pH_2O.

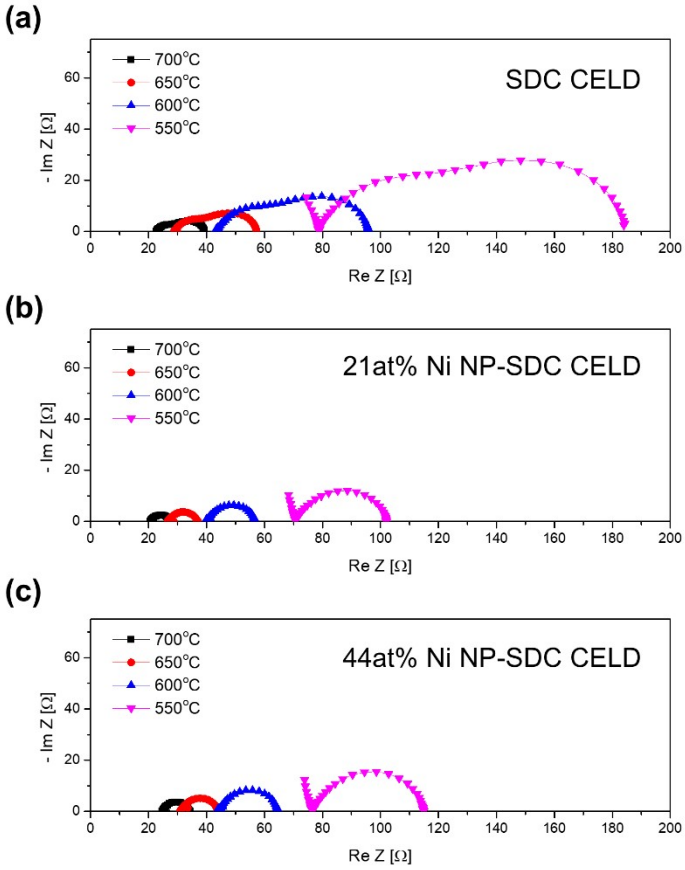

Figure S11. The impedance spectra of SDC CELD, 21at% Ni NP-SDC CELD, and 44at% Ni NP-SDC CELD samples in the measurement temperature range between 550°C and 700°C in 10%H_2-1%H_2O/N_2 atmosphere.

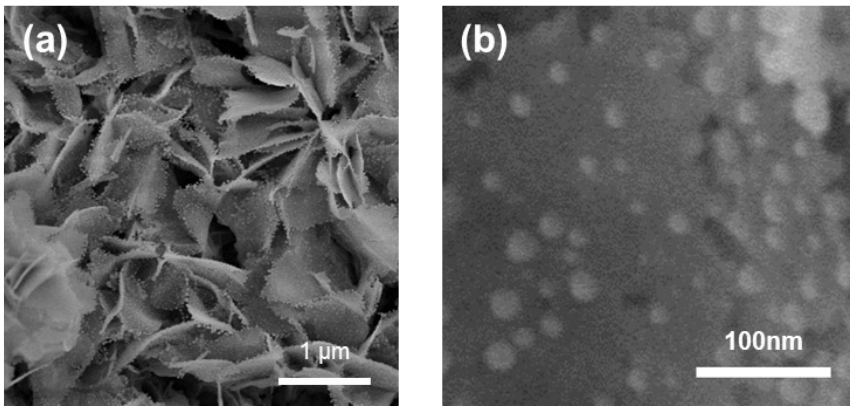

Figure S12. SEM images of 21% Ni NPs-SDC after EIS test under the various wet H_2 measurement conditions.

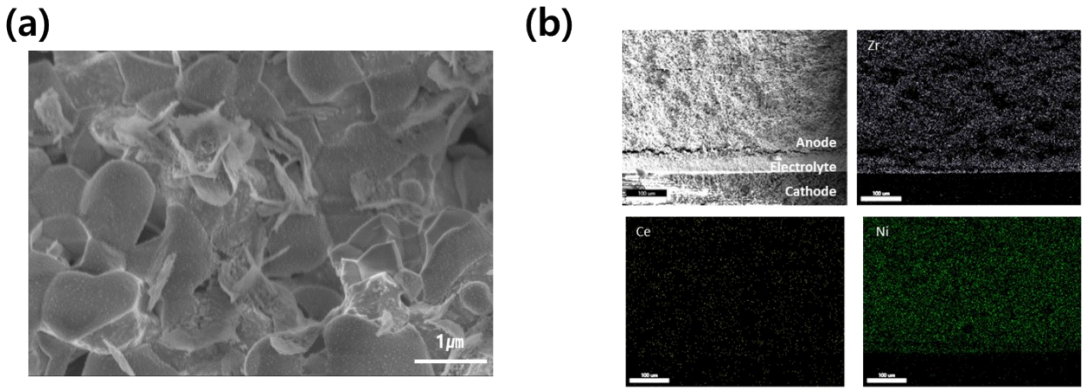

Figure S13. Cross-section SEM images of the Ni NP-SDC coated porous Ni-YSZ composite nanostructures. (a) Coated anode part, (b) overall area, respectively.

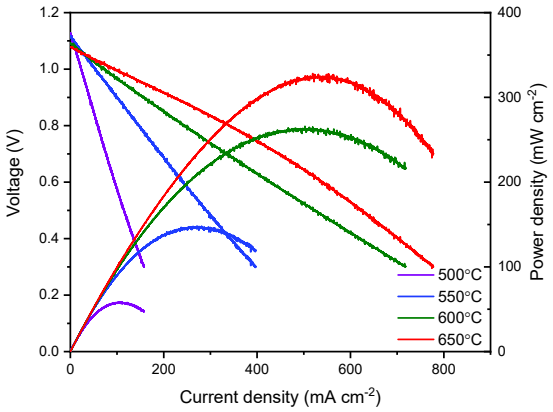

Figure S14. I-V and I-P characterization of Ni-SDC coated full cell under 3%H_2O/H_2 condition.

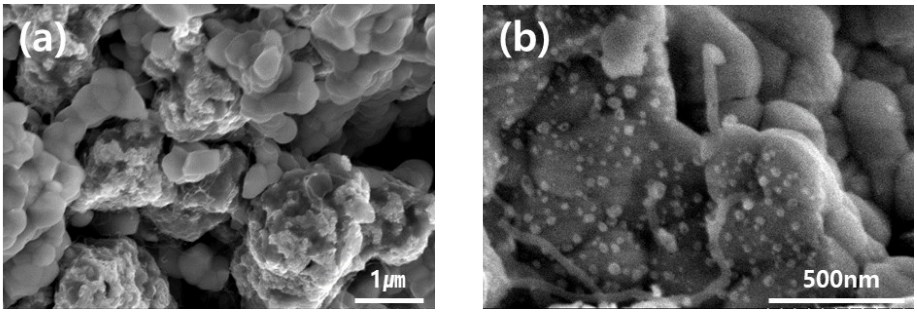

Figure S15. SEM image of the outer region of Ni NP-SDC CELD coated Ni/YSZ after the full cell test under 3%H_2O/H_2 and 3%H_2O/CH_4 at 650^oC.

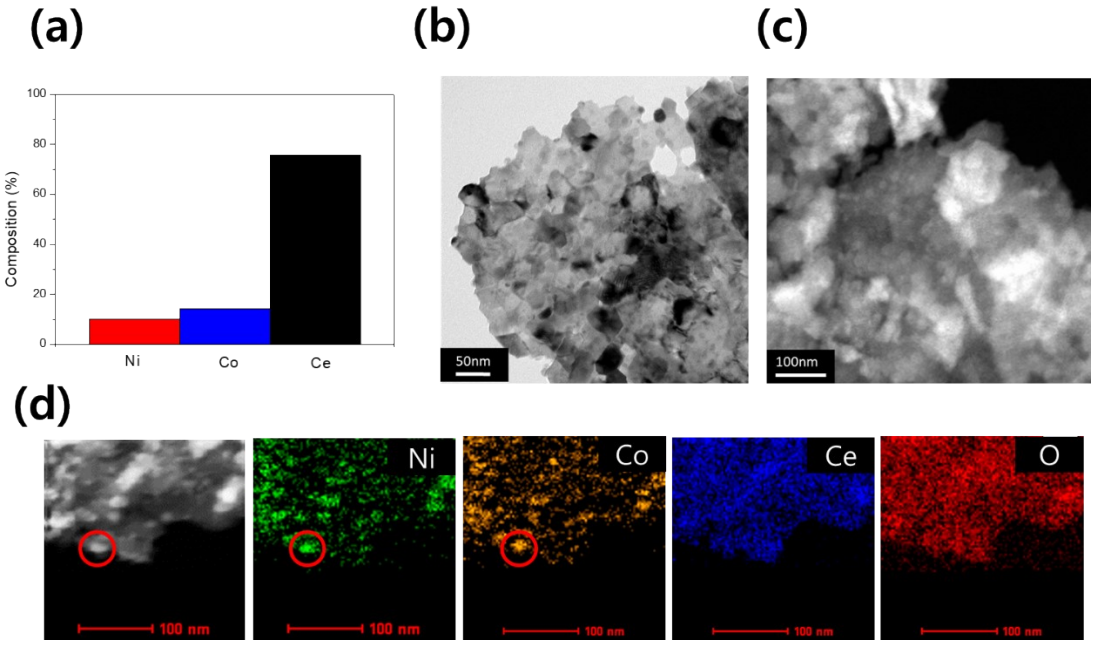

Figure S16. TEM-EDS and XRF data of Ni-Co alloy loaded SDC film.

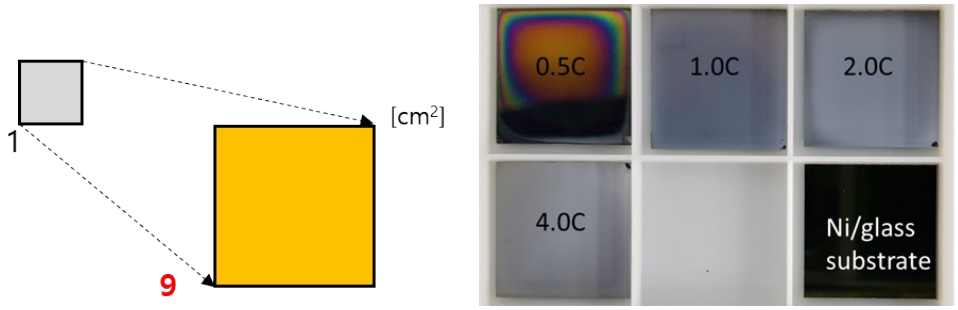

Figure S17. Optical images of Ni-SDC coated 3 × 3 cm^2 Ni/glass substrate.

Reference

[1] E.C. Brown, Ph. D Thesis, Caltech, 2011.